EUROGRAPHICS '98 / N. Ferreira and M. Göbel
(Guest Editors)

*Volume 17, (1999), Number 3*

# Real-time Biomechanically-based Muscle Volume Deformation using FEM

Qing-hong Zhu, Yan Chen, and Arie Kaufman

Center for Visual Computing
and Department of Computer Science
State University of New York at Stony Brook
Stony Brook, NY 11794-4400
USA

**Abstract**

*This paper presents a voxel-based biomechanical model for muscle deformation using finite element method (FEM) and volume graphics. Hierarchical voxel meshes are reconstructed from filtered segmented muscle images followed by FEM simulation and volume rendering. Physiological muscle force is considered and linear elastic muscle models for both static and dynamic cases are simulated by FEM. Voxel-based wireframe, polygon surface rendering, and volume rendering techniques are applied to show real-time muscle deformation processes as well as realistic animations.*

Keywords: *voxel-based, biomechanically-based muscle modeling, real-time muscle simulation, finite element method, hierarchical representation, volume graphics, volumetric deformation.*

## 1. Introduction

Human figure modeling, rendering and animation have been one of the primary areas of research in computer graphics since the early 1970's. In medical applications, such as surgery planning, we are more concerned with how it works as well as what it looks like. As a step to support these applications, we present a new approach which makes use of a sound biomechanical FEM model and voxel-based modeling and rendering.

Our approach involves the following steps:
(1) Set up a hierarchical voxel mesh from a filtered dataset, reconstructed from a sequence of scanned images of the muscle. This is a preprocessing step for building the muscle model (see Section 3);
(2) Employ a 3D voxel-based FEM system with a biomechanical model to simulate both static and dynamic deformations. All deformations are performed interactively on volumetric meshes (see Sections 4, 5);
(3) Apply various volume graphics techniques for real-time rendering of the deformed muscle data (see Section 6).



### 1.1. Anatomy-based vs Biomechanically-based

Recently there has been a trend to model the human figure in an approach similar to the one taken in artistic anatomy - by analyzing the relationship between exterior form and the underlying structures responsible for creating it. Keeve et al.[10] developed an anatomy-based facial tissue modeling for surgical simulation using FEM. However, they only considered a static model, and their nonlinear design is still under development. Scheepers et al.[15] used ellipsoids to represent muscle bellies. They also built models for Fusiform muscles and multi-belly muscles. Wilhelms and VanGelder's model[19] consisted of individual muscles, bones, and generalized tissues covered by an elastic skin. Muscles were considered as deformable objects, discretized cylinders lying between fixed origins and insertions on specific bones.

Despite these innovations, these models lack medical proof and their images are imprecise. Instead, we turned to a biomechanically-based approach. First, we extracted information from a volumetric dataset, such as slices of CT or MRI, through the use of image processing. Then, we used

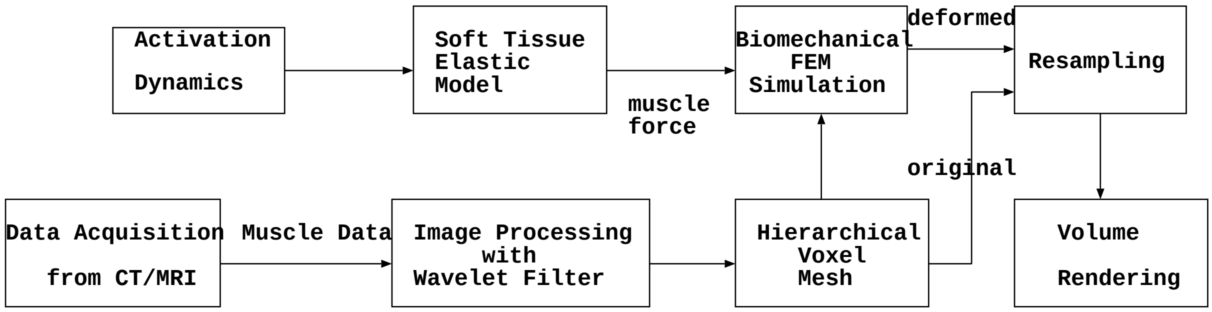


**Figure 1:** Diagram of biomechanically-based muscle volume deformation simulation system

biomechanically-based modeling, in which the behavior of objects is determined via simulations of biomechanical laws and math equations, to determine how bodies move and change shape over time.

Anatomy-based modeling may be useful for entertainment and art, but it is not suitable for medical applications. Biomechanically-based volume visualization, which applies volume graphics to real medical applications – including surgical simulation, treatment planning, and outcome prediction based on scanned images and biomechanical models – can give more appropriate simulation results.

### 1.2. Surface based vs Volume Based

In the computer graphics field, there is growing interest in complex, physically-based models which make deformation and behavior realistic. Most existing models are surface-based, where physical principles are applied to surface primitives or spline control points. However, these surface approaches are insufficient for simulating the effects of manipulation and modeling on object interiors. For example, in surgical simulation, we may wish to visualize a tumor through the surrounding brain tissue or simulate cutting through the deformable brain tissue in order to extract the tumor.

In addition, in many medical applications, there is a need to model both rigid bodies and deformable soft tissues. Voxel-based object models provide a way to represent the interior structure of heterogeneous, deformable tissues. It is also possible to use 3D medical image data directly with this representation, without requiring the extraction of approximate edges and surfaces.

This paper investigates physically realistic manipulation of voxel-based objects. There are several challenges for volume deformation of soft tissue objects. First, we need to build a 3D dynamic model based on plastics theory, which has traditionally proved difficult in biomechanical research for human muscle, and where little work has been executed. The second is speed; the classical 3D elastic model is composed of time dependent partial differential equations which generally need to be evaluated by iteration – a major setback for speed. There are some ways to speed up the process, such as precomputing, using a two-stage dynamic deformation.

### 1.3. Mass-Spring Model vs FEM

Generally, two modeling methods are used for physically-based modeling of the human body: a mass-spring model and FEM model. The mass-spring model is simple and give good, interactive first impressions. However, it is more difficult to control and less accurate than the finite elment method[14].

FEM is a well established engineering method. It is more accurate than the mass-spring model in describing physical deformation. There is growing interest in computer-aided surgery, and in computer graphics and animation in using FEM. Terzopoulos et al.[18] used finite-differences method and FEM in modeling physical deformations based on the elasticity theory. They modeled both rigid and deformable objects and considered physically realistic interactions and animation. The dynamic model produced simulation and animation. Tabatabai et al.[17] presented the principal methods for volume rendering of non-regular grids as used in FEM.

Pieper et al.[14] focused on a system for computer-aided plastic surgery. An automatic mesh generator was used to generate the FE model. For visualizing the FE model, they subdivided the outer face of each element into micropolygons. This method greatly reduced the number of nodes which constitute the FE matrix and thus reduce computational time. Chen and Zelter .[3] simulated a 3D biomechanical FEM. In their model, skeleton kinematics and physiological effect were considered; twenty node brick FEM mesh and a user interface were developed. Apparently, the model is much less accurate in describing and rendering real muscle shape. In both of their systems, volumetric cases were not implemented.

Bro-Nielsen and Cotin [2] introduced condensation, the use of a linear matrix system for simulation and the use of a selective matrix vector multiplication for surgery simulation using FEM. They had achieved real-time volumetric performance for 250 nodes. However, it is difficult to obtain high quality image with such a low resolution.

### 1.4. Hierarchical Volume Graphics

In volume-based modeling, we simulate the physically-realistic behavior of volumetric objects which include many millions of volume elements. For real-time interaction, a fast algorithm is imperative as a basis for trading off between physical realism and speed. This is very challenging work due to the complicated 3D physical model and computational costs, as well as the large memory requirement for computing and rendering. One way is to parallize the execution. Yoo et al.[20,21] implemented multi-valued classification volume renders on a general purpose multiprocessor graphics platform. On the other hand, the multiresolution method or level-of-detail (LOD) can accelerate both the simulation and rendering processes without great loss of image quality. Haley and Blake[8] presented a new algorithm for efficient incremental rendering of volumetric datasets. They used the efficient shear-warp factorization method and represented the volumetric data using a hierarchical data structure which provides for the incremental classification and rendering of volumetric data.

Hong et al.[9] presented an interactive virtual colonoscopy method, using a physically-based camera control model. It is considered as a pioneering work in volume graphics and physically-based modeling, however, their physical models deal with a rigid object which is governed by ordinary differential equations. For soft tissues, we need to develop an advanced elastic model. Gibson[6] proposed the use of a voxel-based data representation not only for visualization, but also for modeling objects and structures derived from volumetric data. More recently, Gibson et al.[5] suggested a 3D chainmail algorithm which enabled fast deformation of volumetric objects. No physical models are included in her algorithms.

For volume rendering of the deformable objects, two methods are used. One method is direct rendering of the curvilinear deformed mesh in the physical space (Mao et al. [11], and Fruhauf [4]). The other approach resamples the curvilinear mesh into a rectilinear grid and subsequently visualizes it with well-developed algorithms for rectilinear data. We used in our system the latter approach.

## 2. System Overview

In the following sections we present a human muscle model that can predict deformation after a force is employed. In contrast to prior approaches, our system is a combination of hierarchical voxel mesh generation algorithms, physically-based biomechanical modeling using FEM, and real-time volume rendering. We demonstrate our system on the human anconeus muscle. The diagram of our system is illustrated in Fig. 1.

In summary, we improve on earlier models in four new ways:

- Implement a biomechanical muscle model which is sound and well recognized by medical experts;
- Generate muscle voxel mesh in level of details, using smoothing Gaussian filter;
- Construct an elastic soft tissue model for muscle deformation; techniques that specify physically-based behavior of both object surfaces and interiors are realized;
- Apply volume graphics and volume rendering on the elastic soft tissue model.

## 3. Biomechanical Model for Muscle Movement

Stern[16] devised a mathematical model incorporating mechanical and physiological parameters of an idealized bone-muscle system, where the movement of a limb is under the action of a muscle. The model considers two aspects of muscle physiology: the effect of shortening (or lengthening) on tension development and the effect of length on tension. His model employs the following assumptions:

(1) At any moment in time during the contraction of a muscle, its exerted force depends only on its level of activation, instantaneous length, and instantaneous velocity of contraction;
(2) The idealized muscle is parallel-fibered, crossing one joint, and with point attachments;
(3) The effort of moving the muscle is disregarded;
(4) The tendon and contractile element are inelastic;
(5) When comparing muscles with different sites of attachment on the moving limb segment, the effect on the moment of inertia of the segment is ignored.

Given the above, the force produced by a muscle at maximum activation obeys the following expression (refer to Fig. 2):

$$P = \left\{ \frac{(P_0)_l/a+1}{\frac{1}{K_i}\frac{1}{(B/C+2+C/B)}\frac{sin(\alpha_i\dot{\alpha}_i)}{j.Y.K_l}+1} - 1 \right\} a \qquad (1)$$

where
$P_0$ = the isometric force at optimum length (i.e. at the length

where isometric force is greatest, hereafter designated by the symbol $L_0$.
$K_i$ = the straight line distance from one attachment to the other (A in Fig. 2) divided by the sum of the distances from the joint to each attachment point (B+C in Fig. 2).
$K_l$ = the value of $K_i$ when the joint is positioned so that the length of the contractile tissue is $L_0$.
$j$ = the value of $b$ expressed in muscle lengths per sec.
a, b = the physiological constant proportional respectively to the cross-sectional area of the muscle and its length.
$\alpha_i$ = the angle between the bones.
$\dot{\alpha}_i$ = the angular velocity of movement.
$Y$ = the fraction of the distance $A$ devoted to contractile tissue when the joint is positioned so that the contractile tissue is at $L_0$.

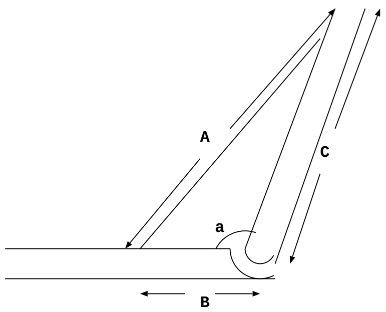


**Figure 2:** Schematic drawing of a parallel-fibered one-joint muscle with point attachments.

Fig. 3 is a 2D image of a cross-section of the arm from Visible Human Dataset (VHD)[12] that includes the anconeus, which is a small and short muscle outside of the elbow joint.

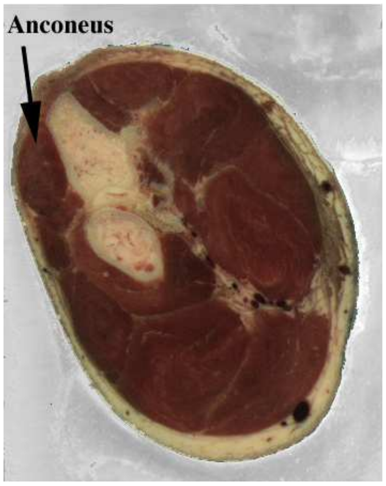


**Figure 3:** Cross-section of the arm from the Visible Human Data which includes the anconeus muscle.

## 4. Building a Hierarchical Voxel Mesh

In this part, image processing techniques and hierarchical methods are used for the generation of voxel meshes. Our data source is the CT anconeus dataset from the VHD. We used 71 slices, with dataset resolution of 140x220x71.

The anconeus muscle image is generated through manual segmentation. Fig. 4(a) shows a muscle image through manual segmentation. The algorithm uses a multi-scale filtering (wavelet) and fuzzy based image segmentation approach. In this method, the wavelet filtering technique[7] is utilized to automatically find the optimal segmentation threshold, and the classification of the image is performed by means of multi-threshold and fuzzy clustering techniques[13]. This method is used to segment the anconeus muscle areas from biceps and triceps of the VHD to reconstruct the 3D muscle volume. Fig. 4(b) uses a ray casting algorithm to show the muscle image obtained from this segmentation method. The muscle voxel meshes are based on the segmented images.

Then, a hierarchical voxel mesh is reconstructed and serves as a multiresolution volumetric approximation of the original muscle data. For each level of detail, first, we read the muscle raw file generated from the manual segmentation, then after filtering, construct the voxel mesh based on the threshold value of the muscle image. The basic operation consists of constructing the voxel mesh inside of the 3D muscle data and giving up other information outside of it. In order to carry out the FEM simulation, we need to build the voxel mesh according to the data structure determined by the FEM simulator which contains 3D geometric coordinates and topology information between each voxel.

In order to obtain a high resolution image, each voxel is recursively subdivided into eight micro-voxels and a hierarchical voxel mesh is thus produced. Based on the different resolution requirement of the application, we construct different level of details of the muscle meshes. Then, we choose one level of resolution that is appropriate to the users' requirements and the computational power of the machine to run the simulation and rendering. As shown in the following sections, we have implemented the static system on all the five levels (refer to Table 1) and the dynamic system on the voxel size of $8\times8\times8$. Because it takes a very long time to simulate high-resolution muscle deformation using 3D FEM, it is advantageous to have muscle shape change in low and medium-resolution and apply FEM simulation on it. With the muscle shape deformation at low or medium-resolution, it is then relatively easy to predict high-resolution deformation image by comparison, mapping and interpolation. Similarity Law[1], which is widely used in engineering design, is used to compare the deformation picture between low and medium-resolution

(a)

(b)

**Figure 4:** Anconeus muscle volume dataset: (a) Surface rendering, (b) Ray casted image of manually segmented anconeus

and high-resolution images. Pieper et al.[14] used another approach by carrying out FEM simulation with a smaller number of nodes and elements and then subdivided each element into micropolygons to create a high-resolution image.

**Table 1:** Hierarchical voxel meshes for both 3D finite element simulator input and volume rendering

| Voxel Size | No of Voxels | No of Nodes | Fixed Points | Loaded Points |
|---|---|---|---|---|
| 16 x 16 x 16 | 28 | 91 | 4 | 4 |
| 8 x 8 x 8 | 219 | 450 | 4 | 4 |
| 4 x 4 x 4 | 1840 | 2664 | 9 | 4 |
| 2 x 2 x 2 | 14578 | 17723 | 11 | 9 |
| 1 x 1 x 1 | 116630 | 128924 | 31 | 22 |

The voxel mesh is used in the rendering as well, so we can integrate real-time simulation and rendering based on the same mesh structure.

## 5. FEM Simulation for Muscle Deformation

We have developed our algorithms for both static and dynamic systems based on elastic theory and finite element principles. In the following, we discuss our FEM algorithms.

### 5.1. Theory

In our model, we assume the muscle is behaving as an elastic soft tissue. We consider it a 3D muscle with an 8-node 3D brick element which is equivalent to the voxel structure in volume graphics. In the problem-solution considered here, the required linear analysis conditions:

- The displacement be infinitesimally small so that the equilibrium of the body can be established with respect to its unloaded configuration;
- The stress-strain material matrix vary as a function of *X, Y, Z*.

To calculate the response of the muscle, we establish the governing differential equations of equilibrium for both the surface and interior of the muscle, which then have to be solved subject to the boundary conditions. In the following, we discuss two basic systems that we used: static and dynamic.

### 5.2. Static System

The linear elastic model can be obtained by the general elasticity equilibrium equation. The effect of body forces is ignored and the system equation can be written as:

$$K\vec{x} = b \tag{2}$$

where $\vec{x}$ is the displacement vector and $b$ is a nodal load vector. The coefficient matrix $K$ is a stiffness matrix. The boundary conditions of the system are given by muscle nodes which belong to the FEM mesh. By solving the linear sparse system we obtain displacements for all the nodes of the FEM mesh. These displacements are implemented into the graphical modeling system. The muscle shape changes can be visualized using different graphical techniques.

### 5.3. Dynamic System

Based on Lagrangian dynamics, the deformable model equations of motion can be expressed in 3D vector form by the second-order ordinary differential equations:

$$M\frac{\partial^2\vec{x}}{\partial t^2}+C\frac{\partial\vec{x}}{\partial t}+K(\vec{x})\vec{x}=\vec{f}(\vec{x},t) \tag{3}$$

where $\vec{x}$ is a 3n vector of nodal displacement, *M, C* and*K* are 3n$\times$3n matrices describing the mass, damping and stiffness between nodes within the volumetric object respectively, and*f* is a 3n vector of forces applied to each node.

The solution of the displacement, velocity and acceleration at time $t+\Delta t$ can be obtained by using center and Euler finite differences written by Lagrangian equation for the full system as:

$$\frac{\partial^2\vec{x}}{\partial t^2}=(x_{t+\Delta t}-2x_t+x_{t-\Delta t})/\Delta t^2 \tag{4}$$

and

$$\frac{\partial\vec{x}}{\partial t}=(x_{t+\Delta t}-x_{t-\Delta t})/2\Delta t. \tag{5}$$

Let's define,

$$K^*=K(x_t)+\frac{M}{\Delta t^2}+\frac{C}{2\Delta t} \tag{6}$$

$$u_t=(x_t-x_{t-1})/\Delta t. \tag{7}$$

$$f^*_{t+\Delta t}=(\frac{1}{2\Delta t}C+\frac{M}{\Delta t^2})x_t+(\frac{M}{\Delta t}-\frac{C}{2\Delta t})u_t+f_{t+\Delta t}. \tag{8}$$

Substituting (4), (5), (6), (7) and (8) for (3), we can obtain,

$$K^*(x_{t+\Delta t})=f^*_{t+\Delta t} \tag{9}$$

Consequently, the explicit procedure evolves the dynamic solution from the given initial conditions $x_0$ and $u_0$ by solving a time sequence of static equilibrium problems for the instantaneous configurations $x_{t+1}$. Thus, the original nonlinear partial differential equations have been reduced to a sequence of sparse linear algebraic equations.

In order to solve the sparse linear system equations quickly, we assume $K^*_t=K$ is time-invariant; thus the matrix decomposition solver need only perform a single initial decomposition of *K*, which significantly reduces the total amount of computation required. Furthermore, the mass matrix and damping matrix are generated at each node by using diagonal damping and mass matrices,

$$M_{ii}=\frac{1}{3}\rho V, C_{ii}=\beta M_{ii} \tag{10}$$

where $\rho$ is the mass-density, $\beta$ is a scaling factor and *V* is the volume.

The algorithm is as follows:

(1) Initial calculations:

- Form 3D brick stiffness matrix *K*, mass matrix *M*, and damping matrix *C*;
- Calculate the initial displacement, velocity and acceleration: $x^0, \dot{x}^0, \ddot{x}^0$;
- Store matrix value in memory;
- Calculate the static deformation based on frontier solver.

(2). Precomputing:

- Select time step size $\Delta t$ and calculate integration constant;
- Derive dynamic difference scheme based on the static deformation and its matrix;
- Store the matrix in the one dimension form using back substitution.

(3). Time loop:

- Calculate new sparse matrix based on the stored matrix;
- Solve for displacements at time $t+\Delta t$ using explicit differential scheme based on the stored matrix values (*K, M, C*);
- Calculate new velocity and acceleration at time $t+\Delta t$.

Our FEM algorithms are integrated with wireframe and shaded polygon graphics so that real-time display is realized in our FEM simulation system. The algorithms are written with C/OpenGL. In the following section, we review several graphical techniques and see how we integrate them together.

## 6. Visualizing Volumetric Muscle Deformation

We have used three visualization techniques to visualize our deformed muscles: wireframe, shaded polygons and volume rendering.

3D wireframe is the fastest but least realistic form of display. Objects are drawn as though made of wire, with only their edges showing. The visible (within the view volume) portions of all edges of all objects are shown in their entirety, with no hidden-edge removal. All edges attributes affect screen appearance in their designated way in this model. We use this model with OpenGL in Fig. 5.

Shaded polygons display filled areas and polyhedra in a more realistic fashion. The addition of shaded areas to the rendering process increases the complexity significantly, because spatial ordering becomes important. Figs. 6 and 9 are rendered by using OpenGL in this way. Both wireframe and polygon shadow models are integrated into FEM routine to create a real-time simulation and display system.

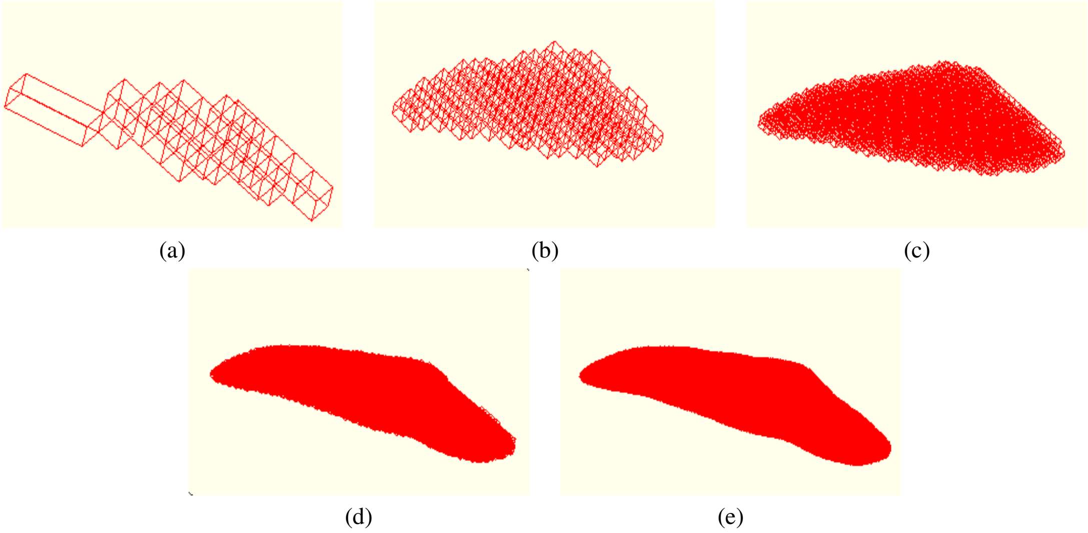


**Figure 5:** Wireframe model for binary hierarchical muscle voxel meshes of different voxel sizes: (a) $16\times16\times16$. (b) $8\times8\times8$. (c) $4\times4\times4$ . (d) $2\times2\times2$. (e) $1\times1\times1$.

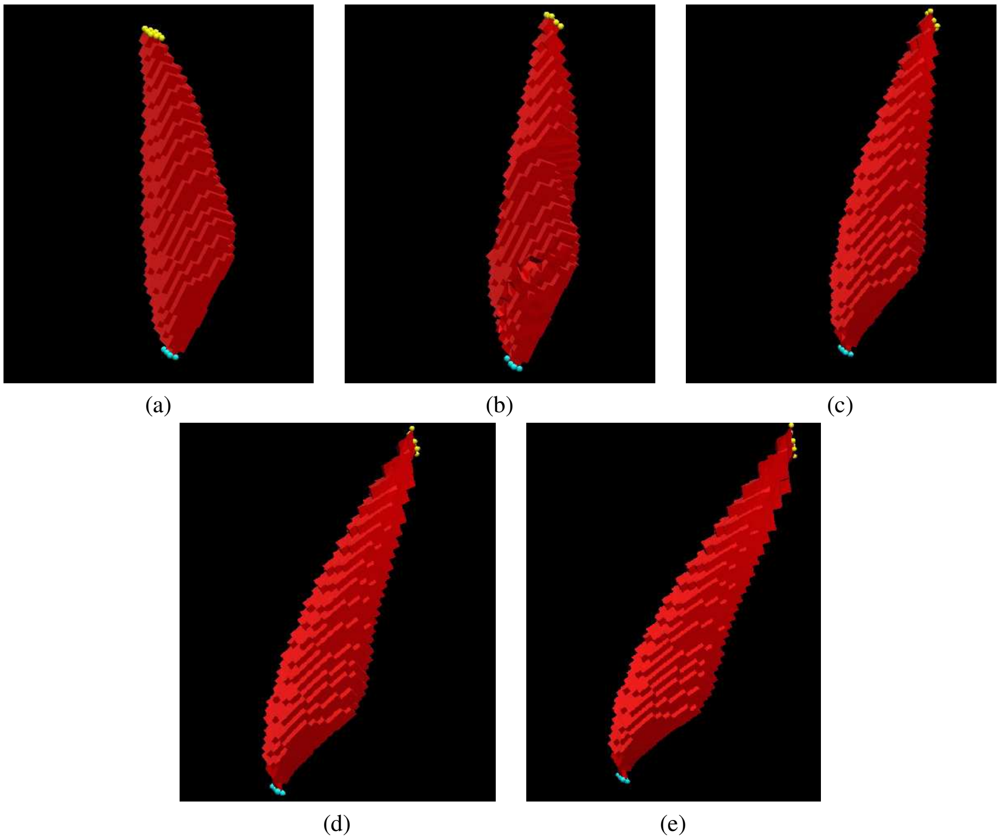


**Figure 6:** Medium resolution of static muscle model: (a) with no Newtons of force applied; (b) with 250 Newtons of force applied; (c) with 500 Newtons of force applied; (d) with 750 Newtons of force applied; (e) with 1000 Newtons of force applied.

Volume rendering is the process of displaying 2D composited images of a 3D scalar field. Here, the scalar field is the density. After deformation, the data are located on a curvilinear grid, and we resample the data at the points of a regular grid. We take the approach of resampling and volume rendering the regular grid instead of directly volume rendering the curvilinear grid. With the condition of FEM linear analysis (Sec. 5.1), the displacement should be infinitesimally small. Thus, the changes in *x, y* and *z* coordinates of voxels are quite uniform, i.e., there is no cells of drastically different sizes and resampling is therefore appropriate. Since resampling can be performed only once with multiple rendering, the whole process is still quite efficient. In our implementation, we compute the isosurfaces as well as display integrals of density along rays by assigning density only to certain isosurfaces, and then ray trace the results (which amounts to creating different volumes to be displayed). Fig. 7 is a filtered image of the original anconeus volume data which includes 14,578 voxels, rendered by ray tracing. We also use it in Fig. 8.

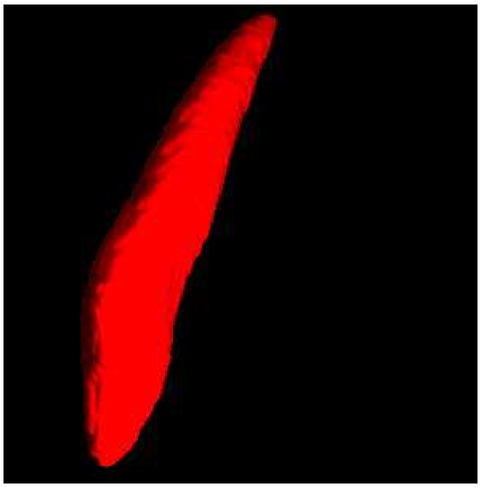

**Figure 7:** Filtered image from voxel meshes of 14578 voxels

## 7. Results

The anconeus muscle from VHD is used as an example to demonstrate our techniques. The simulation and rendering were carried out on an SGI Power Onyx/RE2, R10000, 195MHz, 640MB.

Fig. 5 and Table 1 represent reconstructed hierarchical meshes based on the segmented 3D muscle image. The meshes are constructed with 3D eight-node brick elements which are equivalent to the voxels of volume graphics. The muscle geometrical coordinates and topological information are obtained by this method. Fig. 5 shows the hierarchical muscle voxel model in five different levels of detail with binary increment of the voxel size (refer to Table 1). The meshes produced here can be used for real-time simulation and rendering. The more voxels, the more accurate the muscle image is. However, the FEM dynamic simulation is very slow without preprocessing of the high-resolution muscle mesh. The hierarchical structure is very helpful for predicting real muscle deformation through FEM simulation with low and medium-resolution muscle meshes.

Figs. 6 and 8 show five different muscle images according to different forces applied. The bottom of the muscle (blue points) is fixed, while forces are applied at the top (yellow points) in three directions. The FEM simulation is completely volumetric so that we can see changes of the muscle shape in the various cases. It is very important to both know and view the muscle geometric change imposed by the external force when we carry out surgery simulation and cutting. The images of Fig. 6 were generated using OpenGL shaded polygons with 1,840 voxels, and those of Fig. 8 were produced by ray-casting with 14,578 voxels each.

Fig. 9 presents several snapshots of our dynamic FEM simulation rendered with OpenGL shaded polygons. The dynamic model shows the damping process of the muscle when a sudden external force is applied at the top of the muscle (yellow points) while the bottom (blue points) is fixed at the lowest points. The muscle is oscillating with decreasing frequency. The FEM simulation is carried out with 450 nodes and 219 voxels. The whole process took 0.76 seconds for 22 frames.

## 8. Summary

We have presented a biomechanically-based 3D FEM muscle model which allows accurate prediction of muscle deformation changes. Our reconstructed muscle mesh is based on individual patient CT/MRI volume data. We use a hierarchical voxel mesh which is suitable for both FEM simulation and volume graphics. The physiological muscle force is considered and linear elastic muscle model for both static and dynamic cases are simulated by FEM. 3D wireframe, polygon surface and volume rendering techniques are applied to show real-time muscle deformation processes as well as realistic animation in the low and medium-resolution. The simulations and renderings of VHD anconeus muscle demonstrate the performance of the new approach.

Our future research is directed towards improving the quality and speed of deformed volume rendering. We plan to use the solution obtained from low and medium-resolution simulation as a starting point for the high-resolution simulation and to adapt hierarchical voxel meshes to the complexity of computation on the fly. We also plan to parallelize the simulation and rendering. Another possibility is to use modal

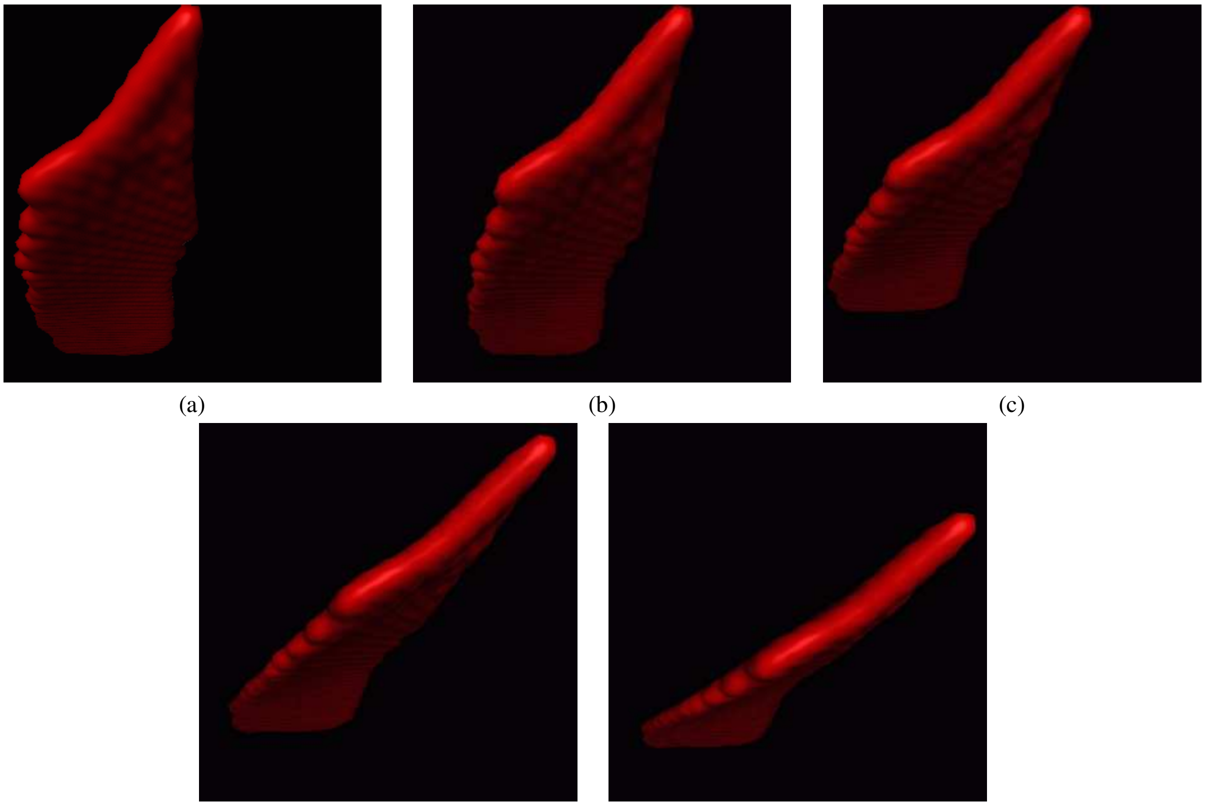

(a) (b) (c) (d) (e)

**Figure 8:** High resolution of static muscle model: (a) with no Newtons of force applied; (b) with 250 Newtons of force applied; (c) with 500 Newtons of force applied; (d) with 750 Newtons of force applied; (e) with 1000 Newtons of force applied.

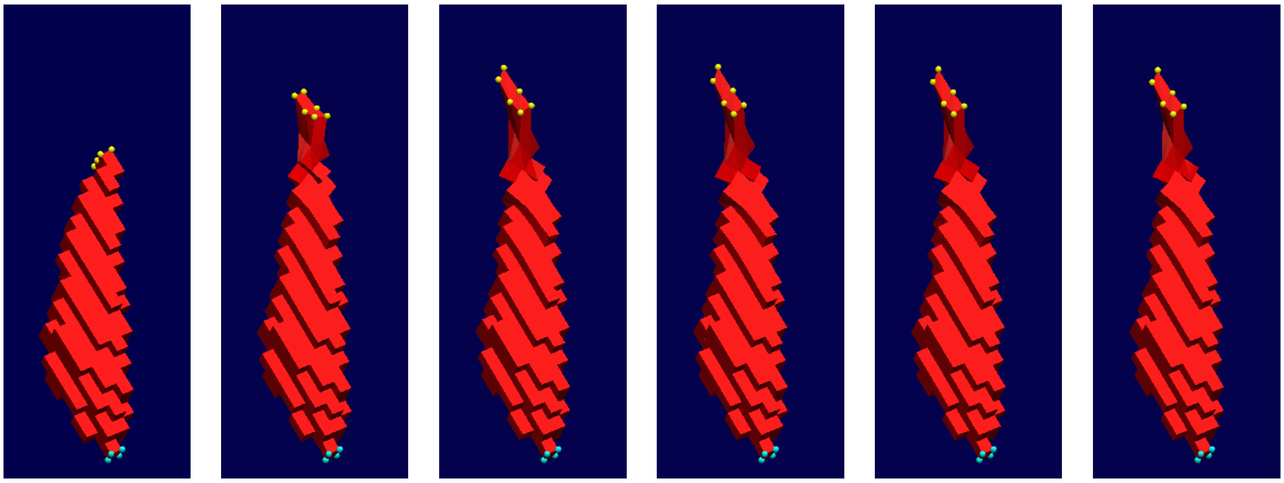

(a) (b) (c) (d) (e) (f)

**Figure 9:** Medium resolution of dynamic muscle model: (a) - (f) from start to end

analysis for FEM dynamic system analysis. While the direct integration method is suitable for a smaller number of voxels, modal analysis is more appropriate for a larger number of voxels.

## 9. Acknowledgments

We would like thank Shigeru Muraki, Suya You, Ming Wan, Akio Doi and Ikuko Takanashi for their earlier work on this project. Also, thanks to Jeffrey Ge and Jack Stern for their useful suggestions for our work. Kathleen McConnell advised us greatly in writing this paper. Pat Tonra and Ken Gordon also provided much help. The project was partially supported by Mitsubishi Electric Research Lab (MERL) and Office of Naval Research (ONR) under grant N000149710402, and National Science Foundation (NSF) under grant MIP-9527694..

*References:*

1. Bisplinghoff, R. L., Ashley, H. and Halfman, R., *"Aeroelasticity"*, Addison-Wesley, 1955.

2. Bro-Nielsen, M., and Cotin, S., "Real Time Volumetric Deformable Model for Surgery Simulation using FE and Condensation," *Proc. Eurographics '96* pp.C57–C66.

3. Chen, D., and Zeltzer, D. "Pump It Up: Computer Animation of a Biomechanically Based Model of Muscle Using the Finite Element Method," *Proc. Siggraph'92*, pp.89-98.

4. Fruhauf, T., "Raycasting of Nonregularly Structured Volume Data," *Proc. Eurographics '94*, pp. 293–303.

5. Gibson, S.F.F., Samosky, J., Mor, A., Fyock, C., Grimson, E., Kanade, T., Kikinis, R., Lauer, H., McKenzie, N., Nakajima, S., Ohkami, H., Osborne, R., Sawada A., "Simulating Arthroscopic Knee Surgery using Volumetric Object Representations, Real-Time Volume Rendering and Haptic Feedback", MERL Tech Report TR96-19

6. Gibson, S.F.F., "Beyond Volume Rendering: Visualization, Haptic Exploration, and Physical Modeling of Voxel-based Objects," *Eurographics Workshop on Visualization in Scientific Computing*, 1995, pp. 171–201.

7. Grosso, R. and Ertl, Th., "Biorthogonal Wavelet Filters for Frequency Domain Volume Rendering", *Visualization in Scientific Computing '95*, pp. 81-95.

8. Haley, M., and Blake, E. H., "Incremental Volume Rendering Using Hierarchical Compression, " In *Proc. Eurographics '96*, pp. 45–55.

9. Hong, L., Muraki, S., Kaufman, A., Bartz, D., He, T., "Virtual Voyage: Interactive Navigation In The Human Colon," *Proc. Siggraph '97*, pp. 27–34.

10. Keeve, E., Girod, S., Pfeifle, P., Girod, B., "Anatomy-Based Facial Tissue Modeling Using the Finite Element Method," *Proc. IEEE Visualization '96*, pp. 21–28.

11. Mao, X., Hong, L. and Kaufman, A., "Splatting of Curvilinear Volumes", *Proc. IEEE Visualization '95*, pp. 61-68.

12. National Library of Medicine, "The Visible Human Project", *with URL: http://www.nlm.nih.gov/research/visible/visible_human.html, 1997*.

13. Nguyen, H. H. and Cohen, P., "Gibbs Random Fields, Fuzzy Clustering, and the Unsupervised Segmentation of Textured Images", *Computer Vision, Graphics, and Image Processing. Graphical Models and Image Processing*, January 1993, 55(1), pp. 1-19.

14. Pieper, S., Rosen, J. and Zeltzer, D., "Interactive Graphics for plastic Surgery: A Task-level Analysis and Implementation," *1992 Symposium on Interactive 3D Graphics*, pp. 127–134.

15. Scheepers, F., Parent, R., Carlson, W. and May, S., "Anatomy-Based Modeling of the Human Musculature" *Proc. Siggraph '97*, pp. 163-172.

16. Stern, J., "Computer Modeling of Gross Muscle Dynamics," *Journal of Biomechanics*, 1974, Vol. 7, pp. 411-428.

17. Tabatabai, B., Sessarego, E. and Mayer H., "Volume Rendering on Non-regular Grids," *Proc. Eurographics '94*, pp. C247–C258.

18. Terzopoulos, D., Platt, J., Barr, A. and Fleischer, K., "Elastically Deformable Models," *Proc. Siggraph '87*, pp. 205–214.

19. Wilhelms, J. and Van Gelder, A., "Anatomically Based Modeling," *Proc. Siggraph '97*, pp. 173-180.

20. Yoo, T., Neumann, U., Fuchs, H., Pizer, S. and Cullip, T., "Direct Visualization of Volume Data", *IEEE Computer Graphics and Applications*, 12(4), pp. 63-71, July 1992.

21. Yoo, T., Neumann, U., Fuchs, H., Pizer, S., Cullip, T., Rhoades, J. and Whitaker, R., "Achieving Direct Volume Visualization with Interactive Semantic Region Selection", *Proc. IEEE Visualization '91*, pp. 58-65, 1991.